DOI: 10.13009/EUCASS2022-4848
9TH EUROPEAN CONFERENCE FOR AERONAUTICS AND SPACE SCIENCES (EUCASS)

Shock Wave Reflection from Plasma Array

Sergey Leonov, Philip Andrews, Philip Lax*
Institute for Flow Physics and Control, University of Notre Dame, USA
*109 Hessert Lab, Notre Dame, IN, 46556, USA, * sleonov@nd.edu*

Abstract
This work is focused on shock wave - boundary layer interaction (SWBLI), pressure redistribution along a rectangular duct, and dynamics of a supersonic M=2 airflow structure under the impact of surface generated, transient energy deposition in a shock-dominated airflow. The power deposition is provided by means of a Quasi-DC electrical discharge, which generates a filamentary plasma between flush mounted surface electrodes arranged in a spanwise array. The test arrangement includes a shock wave (SW) generator installed on one wall of the test section and a plasma generator installed on opposite wall. The SW impinges upon the disturbed boundary layer (BL) with a stripwise zones of elevated temperature generated by the plasma array. The effect of reflected SW mitigation is demonstrated due to the interaction with the plasma-modified BL. The model of interaction is discussed along with prospects for implementation in practical systems.

1. Introduction

Study of the Shock Wave – Boundary Layer Interaction (SWBLI) is one of the major trends in state-of-the-art fluid dynamics. Supersonic inlets, scramjet isolators, profiled supersonic ducts represent the relevant configurations just listing a few. The shock-dominated flow structure is typically sensitive to small fluctuations in parameters of incoming flow and wall conditions making the detailed prediction and accurate control challenging [1, 2, 3, 4]. Another important aspect of the SWBLI control is hysteresis in the shock-dominated flow structure dynamic response such that the time of the control system actuation is matter. An example of system hysteresis is supersonic inlet unstart: once completed, it is difficult to restore it to its original state.
Three main components are involved in the Process of SWBLI: impinging/reflected SWs, incoming BL (turbulent BL in the case considered here) and a SW-induced separation zone resulting from a reversal gradient of the wall pressure. It is commonly suggested that the most effective mechanism leading to the prevention of flow separation, is the formation of streamwise vorticity, which transfers gas momentum from the core flow to the BL [5, 6]. For this purpose, mechanical elements or steady-state thermal sources are introduced to the flowfield, producing stationary forcing of the flow and generating steady-state SWs with a predefined location in a supersonic flow [7, 8, 9, 10, 11]. Basically, rapid near-adiabatic heating results in an abrupt pressure jump in the zone of heat deposition which acts similar to a mechanical obstacle. Problems with the mechanical methods and gas injection include a lack of flexibility, increased total pressure losses and, frequently, longer response times, orders of magnitude longer than the characteristic gasdynamic time. In these terms, electrical discharge generation inflow looks significantly more beneficial compared to the mechanical methods [12, 13, 14, 15, 16, 17].

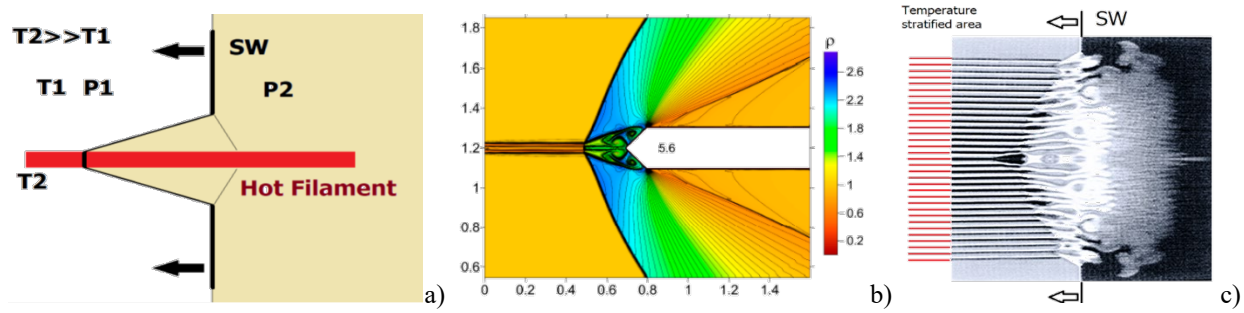

Figure 1: About the mechanism of SW interaction with thermal inhomogeneities. (a) schematics; (b) SW structure in front of blunt body with thermal filament [18]; (c) SW interaction with thermally stratified zone [19].

DOI: 10.13009/EUCASS2022-4848

The mechanism of interaction and consequences of SW propagation in a temperature-stratified media were discussed in several computational works, in Refs. [20, 18, 19] for example. In the presence of a single heated gas filamentary zone, the SW front propagates far upstream compared to the SW in a cold gas due to a higher sonic velocity in the heated zone, as demonstrated in Fig. 1a. In the case of a heated filament realized in front of a blunt body in a supersonic flow, the SW structure significantly modified causing the drag reduction effect, see Fig. 1b. For a multifilamentary heated zone, shown in Fig. 1c, or a "thermally stratified" media, the SW structure looks different compared to a single filament with the SWs forming a quasi-front of the propagating pressure jump. Such a gas heating pattern promises benefits in terms of the energy magnitude needed for the expected control effect. However, a practical realization of a thermally-stratified zone is challenging, especially in a free space [21, 22, 13].
The creation of near-surface electrical discharges in a supersonic flow is far more technically reasonable than that of a localized one in free space. The importance of plasma non-uniformity and its transient behavior for SW and BL control has been considered in numerous publications: one of the most recent review papers can be found in [23]. Localized heating generated by the plasma produces "hot spots" operating similar to solid obstacles, although this interpretation may well be too simplistic. In [24, 25], the authors demonstrated the control of an oblique SW position and angle (intensity) by means of an electric discharge between flush-mounted electrodes installed in front of the ramp in a M=2.2 airflow. A significant effect of arc plasma on the ramp pressure distribution was measured in works [26, 27]. The authors of the current paper published the results of several studies related to control of SW structure [28, 29, 30, 31]. These previous studies used a filamentary plasma to demonstrate pressure redistribution due to presence of longitudinal subsonic zones induced by individual plasma filaments.
Plasma-based techniques have been explored in terms of the feasibility for steady or transient SW generation in supersonic flow [32, 29]. This suggests that rapidly heated regions located near aerodynamic surfaces could be used to control the pressure distribution in a variety of aerodynamic configurations. The mechanism of near-surface plasma-flow interaction was discussed in Refs. [28, 17, 30, 33]. In fact [28], the plasma zone presents a set of longitudinal subsonic semi-cones surrounded by a supersonic flow, as is shown in Fig. 2a for a single plasma filament. The volumetrically expanded zone produces a cone of a subsonic flow, where the physical velocity may be close to the gas speed in the core flow. The gas expansion induces the conical SW attached to the plasma filament root (electrode). In the case of a multi-filament plasma array, Fig. 2b, an interference of the conical shock waves produces a combined compression wave attaining the form of a plane shock with a steady shape despite the transient nature of the plasma. Such a unique structure of the near-surface gas layer, consisting of intermittent lengthwise zones of supersonic and subsonic flow due to a non-homogeneous heating in cross-flow spanwise direction, Fig. 2c, possesses a mitigating effect on an external impinging SW [34]. The mechanism of interaction is considered as follows: the pressure increase due to the impact of the impinging SW affects the whole subsonic area, increasing the gas pressure in the upstream zone and reducing the pressure magnitude immediately after the SW.

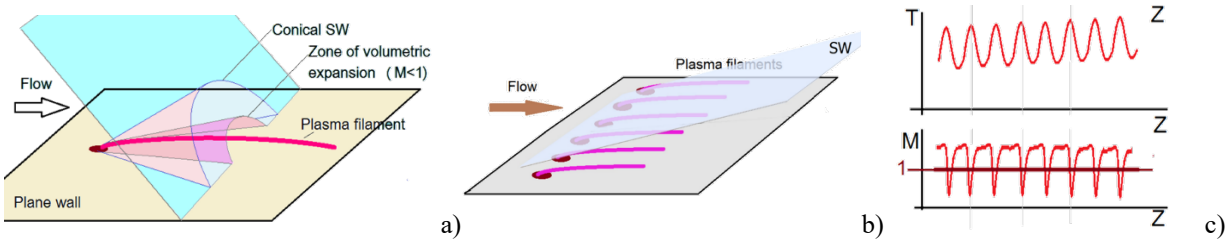

Figure 2: Schematics explaining the mechanism of near-surface filamentary plasma interaction with supersonic flow.

Current work aims to investigate the effect of the plasma array on the reflection of impinging SW in more detail, including the dynamics of interaction and pressure redistribution in vicinity of the shock-induced separation zone.

2. Test arrangement and instrumentation

The experiments were performed in the supersonic blow-down wind tunnel SBR-50 at the University of Notre Dame [35]. The test section is arranged inline with a Mach 2 nozzle. In the current experimental series the conditions were as follows: initial Mach number M=2; total pressure P_0 = 1-3 bar; stagnation temperature T_0 = 300 K; duration of steady-state aerodynamic operation is about t = 1 s. The upper wall of the test section was arranged with a 10degree wedge with a height of 6.6mm to generate a planar shock impinging in the plasma region on the bottom wall, see Fig. 3a. The wedge position is adjustable in a streamwise direction to have the SW on the bottom wall to hit at different locations with respect to the plasma filaments. The plasma was generated using a quasi-DC (Q-DC) electric discharge [28] from three high voltage electrodes embedded in ceramic insert spaced 19mm apart from each other and from the side walls and located 149mm downstream of the nozzle exit. Two grounding rails of width 2.6mm were placed 19.05mm apart from each other and 28.5mm from the side walls in order to elongate the plasma filaments as shown in

DOI: 10.13009/EUCASS2022-4848

Fig. 3b. Plasma was generated using a custom capacitor-based power supply operating in a current stabilized mode at breakdown voltages in a range of Ups = 4-5kV. Electrical probes were used to measure gap voltages, current and, then, to calculate electrical power deposition. Typical electrical parameters for each filament include gap voltage Upl = 0.1-0.3 kV, current around I=4.5A and plasma power about Wpl = 0.8 kW. Optical access was provided through quartz side windows.

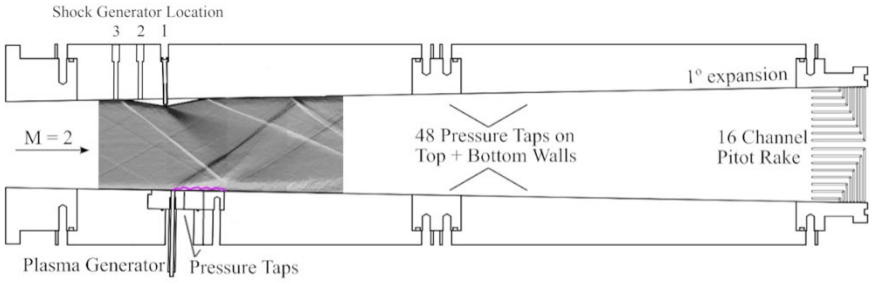

a)

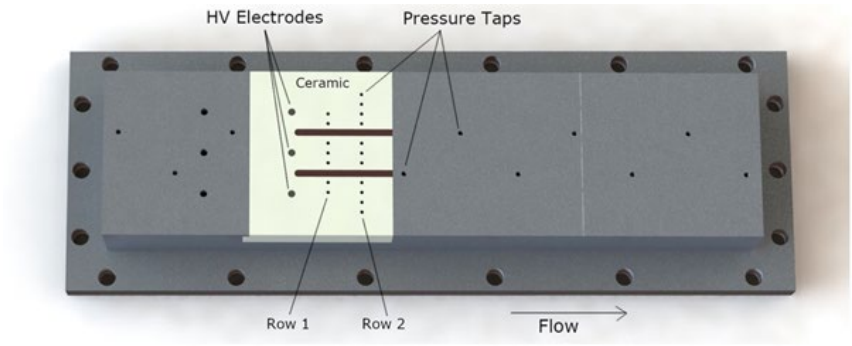

b)

Figure 3: SBR-50 facility test arrangement where (a) shows an overview of the test section and (b) shows an image of the electrode arrangement on the bottom wall.

Instrumentation included pressure sensors, schlieren system, high speed plasma imaging, and electrical measurements. Static pressure data over the test section are measured using a 64-channel pressure scanner (Scanivalve MPS4264) with an acquisition frequency of 800Hz collecting from 48 pressure locations on the top and bottom walls. Pressure measurements are also taken across a span perpendicular to flow along the bottom wall in the plasma generation region to investigate the effect of generated plasma on the 3D flow structure. Two rows of pressure taps at 165.5mm and 180.7mm downstream from the nozzle with 4.57mm spacing between each tap recorded the crossflow static pressure. Kulite pressure sensors with a sample rate of 80000samp/sec were also installed at key locations in the top wall in the vicinity of the reflected shock impact to study the dynamics of shock movement. The schlieren arrangement consists of a high current pulsed white LED light source (100ns pulse duration) and a Photron Nova S9 FastCam high speed camera operating with a framerate of 1kHz and exposure of 1.25μs. Plasma imaging was performed with the Photron Nova S9 FastCam collecting with an exposure of 12.5µs and 20kHz framerate.

The details of the SW structure over the plasma zone is visualized using a Mie scattering technique. For Mach 2 flow, the flow was seeded by lowering the stagnation temperature of the acetone seeded gas until the acetone condenses, forming acetone nano/micro-droplets. Bulk seeding with acetone of the SBR-50 working gas is performed by adding pressurized liquid acetone to a pure N2 stream via liquid atomizer. The mixture is first passed through a static mixer with internal baffles and then a small cell with sapphire windows. Acetone concentration is measured by UV absorbance using a 2 mW 280nm UV LED with collimation and focusing optics and a GaP photodiode combined with a pressure transducer and a resistance temperature detector (RTD). Acetone is seeded at 1-3% by volume. Laser excitation is performed using a ns-pulsed Nd:YAG laser (Solar Laser Systems LQ 629-100) at a 100Hz repetition rate. After frequency doubling from 1064 nm to 532 nm, the pulse energy is approximately 70 mJ/pulse as measured by a thermopile power meter (Ophir 50A-PF-DIF-18). Sheet forming optics are then used to produce a 76mm wide laser sheet that is approximately 200 μm thick at the sheet waist within the test section.

DOI: 10.13009/EUCASS2022-4848

3. Results of measurements and observations

3.1 Plasma morphology

Figure 4 presents a comparison of fully developed plasma filaments' shape for the three filament case and the case when just one filament is activated. The SW is either turned off (the wedge is removed from the test section) or is generated by the ramp and impinging onto the plasma actuation region. Results consistently demonstrated that with this impinging SW present, the plasma filaments are highly perturbed from their otherwise linear shape. This happens due to presence of a flow separation zone as a result of the impinging SW and plasma interaction. The single filament can elongate by grounding to either rail or to the downstream metallic wall and thus its exact position at a given time is largely stochastic, compare Figs. 4a and 4b.

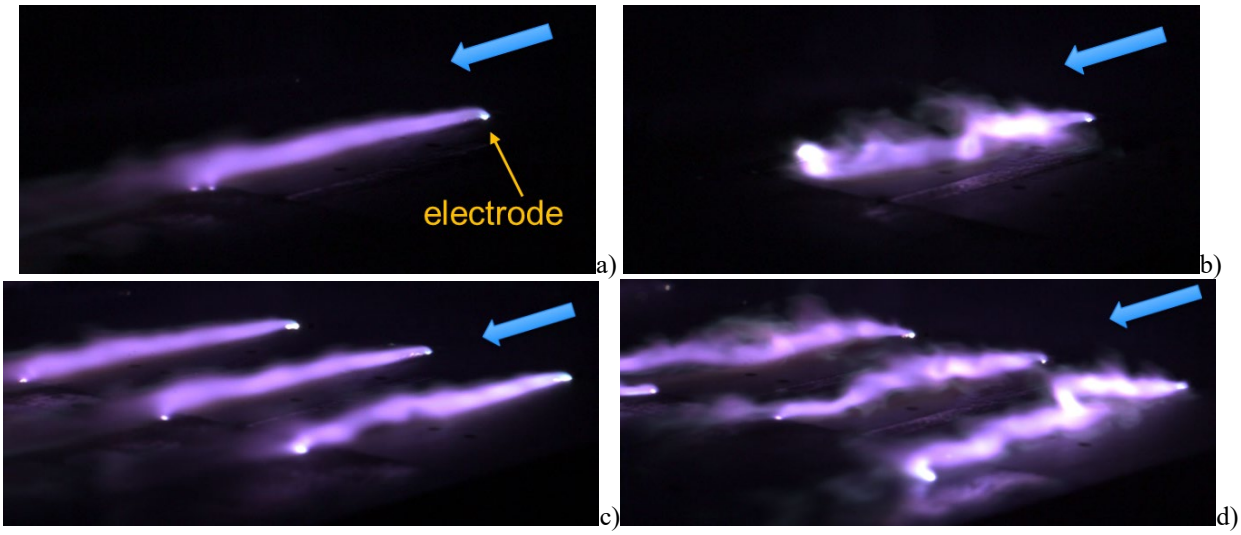

Figure 4: Plasma images, view from top-downstream direction, collected at 20kHz and a 6μs exposure: (a-b) single filament; (c-d) three plasma filament; (a, c) – no SW; (b, d) – SW on.

The plasma morphology is significantly affected by the impinging SW location, as it is demonstrated in Fig. 5. General tendency is that the plasma filament is shortened due to the high pressure zone impact: the length depends on the SW position, compare Figs. 5 a-c-e-g. Another modification is the shape of the plasma filament which often moves off of the surface due to the presence of the recirculation zone, see Fig. 5d for example. Finally, the electrical discharge can frequently switch from a long filament mode to the shorter one. This switching is well reflected in the electrical discharge voltage, as it is shown in Fig. 6, as a longer plasma filament corresponds to a higher gap voltage. At shorter plasma filament, the gap voltage decreases on about 20%, the plasma power decreases proportionally as well. The voltage waveform is highly variable at SW impingement indicating an unstable plasma filament behaviour.

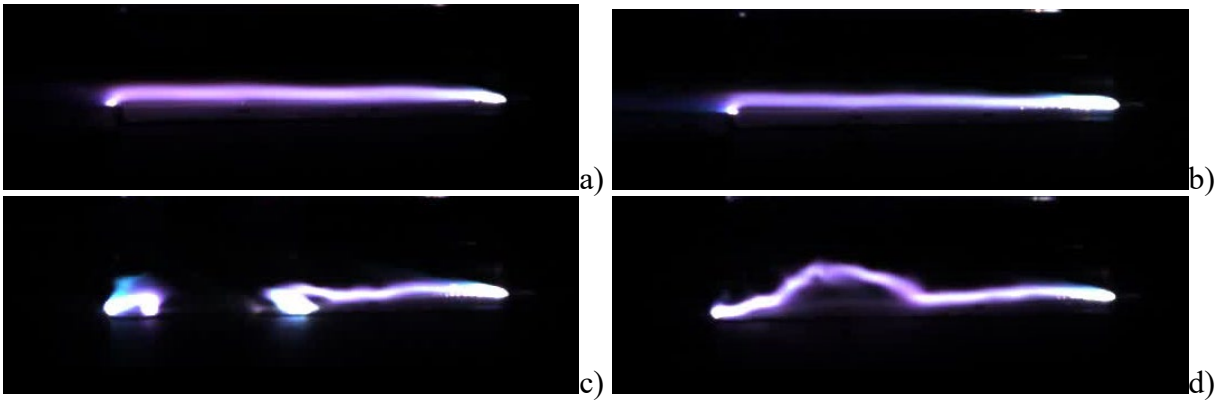

DOI: 10.13009/EUCASS2022-4848

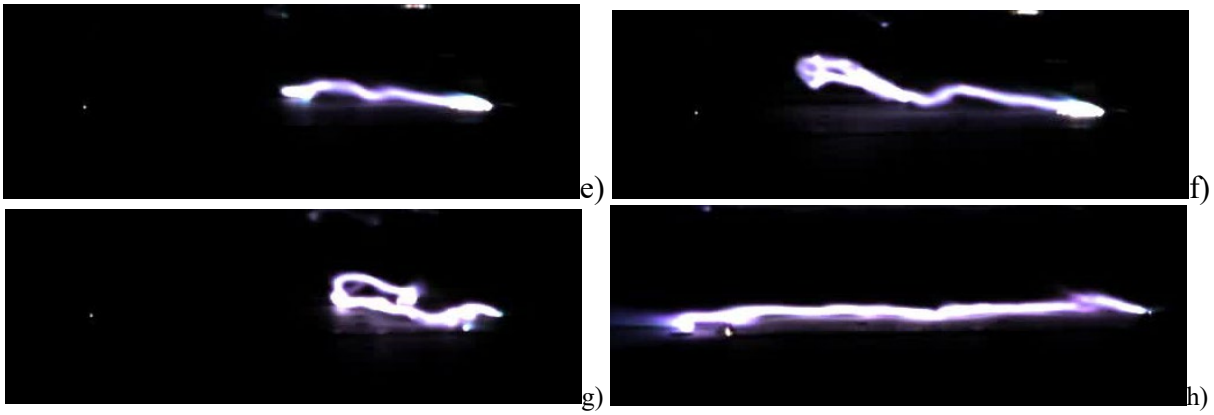

Figure 5: Single plasma filament images at variable SW position, view from side. Left and right columns show different modes of plasma connection: (a-b) SW off, P_0=1.3bar (a) and 2.6bar (b); (c-d) SW at the end of plasma filament; (e-f) mid position; (g-h) near electrodes impinging SW position.

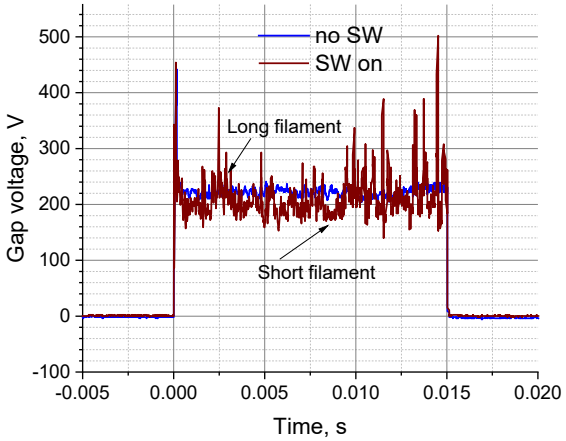

Figure 6: Single plasma filament voltage measurements: no SW vs the impinging SW on at mid position.

3.2 Schlieren visualization

Figure 7 presents schlieren images collected at 1kHz with a 100ns effective exposure time. Images compare the SW off flow, plasma off and on in Fig. 7a, and the impinging SW on at three filament plasma configuration, plasma off and on in Fig. 7b. Without the shock wave generator installed, the SW associated with the plasma is weak, resulting in a few percent of the wall pressure increase [28]. The angle of this SW is practically equal to the Mach angle $\alpha=arcsin(M^{-1})\cong\pi/6$. The situation is significantly different when the SW generator is installed, Fig. 7b. Prior to plasma activation, the flow field is dominated by a strong shock from the leading edge of the compression wedge and the end shock from the ramp back wedge. The basic effect of plasma actuation on the shock train generated by the ramp and on the flowfield structure is seen in schlieren images in two key regions: (1) compression wedge shock impact on the plasma array and (2) the reflection of this shock back to the upper wall. The first reflection of the leading edge oblique shock from the bottom wall is seen near the center of Fig. 7b, at about x=175mm. After extended plasma forms on the bottom wall, the reflection of the shock impinging on the plasma array is largely mitigated. A new shock forms upstream at the location of the high voltage electrodes as demonstrated in Fig. 7b at about x=150mm. This causes an upstream movement of the entire shock train as proven in further detail in previous experiments [31]. With actuation of a single plasma filament, the reflected shock is only partially mitigated and a weak SW is established starting at the electrodes.

DOI: 10.13009/EUCASS2022-4848

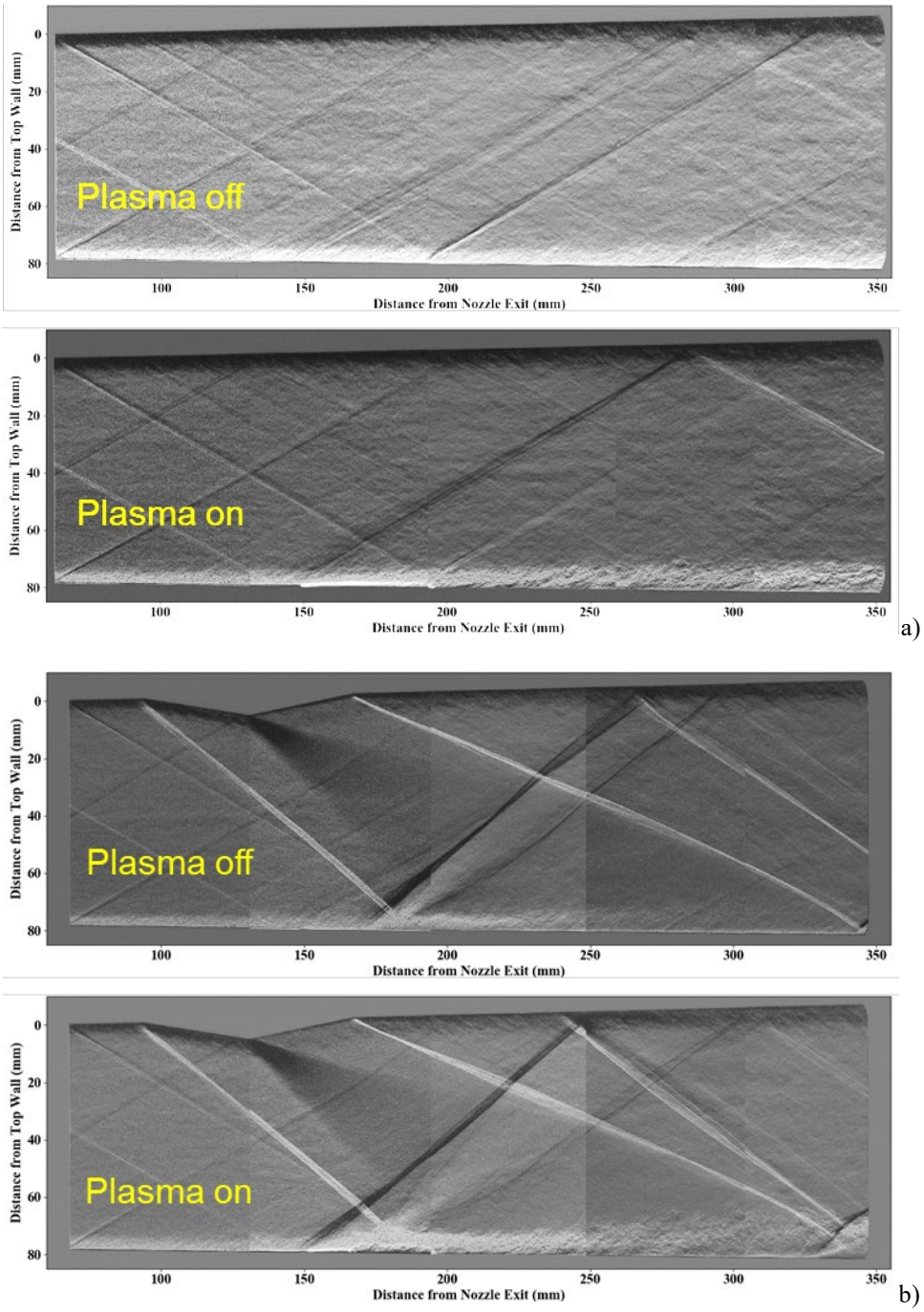

Figure 7: Schlieren visualization of SWBLI: (a) no SW, at 3 filaments plasma array off and on; (b) the impinging SW on at mid position, plasma off and on. Each schlieren image is combined from up to 5 individual frames due to a limited aperture of the schlieren optical system.

3.3 Pressure effect

The effect of plasma on shock structure configuration is well reflected in pressure data taken from the two rows of pressure taps arranged perpendicular to the flow as well as static pressure ports along the top wall. By looking at key pressure ports along the top wall where the reflected shock is impinging, pressure data can corroborate the movement of the shock train displayed in schlieren images. As the reflected shock impacting the top wall moves upstream due to plasma actuation, the pressure at x = 252 mm on the top wall dramatically increases indicating this sensor now locates behind the new shock front [31]. Likewise, examining the two perpendicular rows of sensors in the plasma region

DOI: 10.13009/EUCASS2022-4848

reveals a movement of existing shocks upstream and can also reveal cross-sectional structure for the single filament case.

Figure 8 provides a comparison of crossflow pressure profiles for three positions of the shock generating ramp in the case of a baseline flow vs. plasma actuation. Plasma off pressures are taken during baseline flow just before plasma is turned on and "plasma on" images are based on times of peak pressure disturbance while plasma is on. In Figure 8a, both rows of pressure taps are situated in front of the impinging SW. When plasma is actuated, rapid near-adiabatic heating creates a localized subsonic region which causes an upstream movement of the pressure bump and corresponding SW so that a new shock is generated starting at the plasma location. Thus, pressure taps in both rows are now behind the new shock and exhibit increased pressure primarily along the centerline in the region local to the single filament. In the case of Figure 8b, the first row of pressure taps is still positioned upstream of the impinging SW but the second row is behind the SW which explains the pressure disparity between the two rows before plasma is turned on. After plasma actuation, the pressure profile of the upstream row matches the previous case as expected, but the downstream row now exhibits a decrease in pressure along the centerline due to the upstream movement of air. In Figure 8c, both rows of taps are behind the impingent shock before plasma is turned on, and thus pressure in both rows decreases when plasma causes the SW to move upstream.

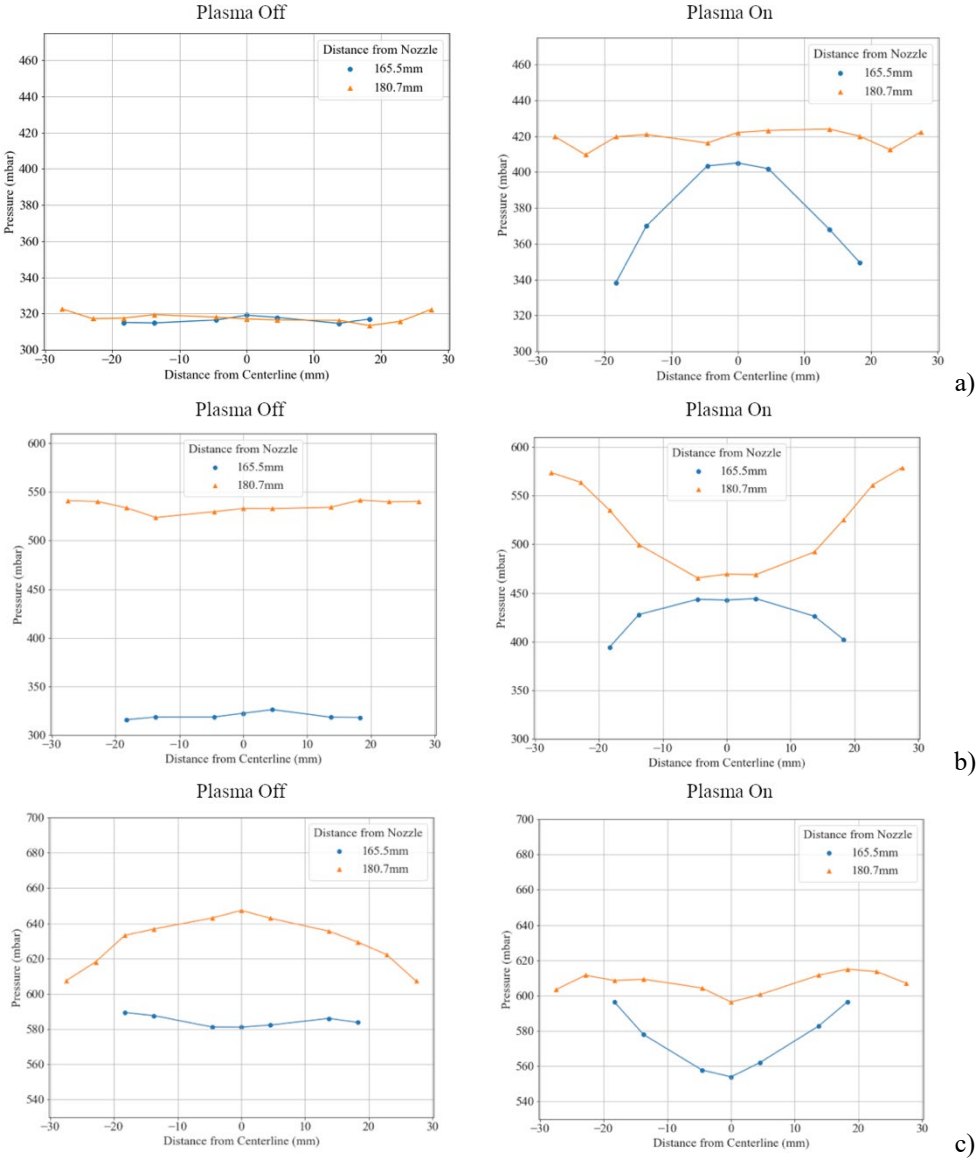

Figure 8: Pressure scanner data at P_0 = 2.6bar comparing baseline flow to plasma actuation for (a) ramp position 1 – furthest upward; (b) ramp position 2; (c) ramp position 3 – furthest downward.

DOI: 10.13009/EUCASS2022-4848

3.4 Mie scattering SW visualization

To further characterize the effect that a single filament has on the shock structure, Mie scattering was used as a way of generating a planar flow visualization. Several different laser sheet locations were recorded to compare three filament operation to single filament modes. Data collected by placing a streamwise sheet along the test section centerline provided excellent agreement with schlieren images, demonstrating upstream movement of the reflected shock in both three filament and single filament cases. The most interesting laser sheet location, however, was aligned with the upstream row of pressure taps at x = 165.5mm from the nozzle. The camera was positioned at a shallow angle to the laser sheet and a projective transform was applied to images later on based on a regular reference grid. Using this transformation, the cross section of SWs profiles was accurately investigated. Since the intensity of Mie scattering is based on the density of condensed droplets, shocks appear as brighter lines. Additionally, increasing the flow temperature can cause acetone to re-evaporate which is why scattered light is absent in the boundary layer and plasma region. Figure 9 provides a comparison between the three filament and single filament shock structures in the plasma region. In the images, the horizontal shock seen on top is the originally impinging shock and the shock visible below is the profile of the reflected shock after behind shifted upstream. With three filaments, the effect of localized heating of each individual filament overlaps each other the new shock is close to linear. With only a single filament, the conical cross section of the new shock is seen in Figure 9b.

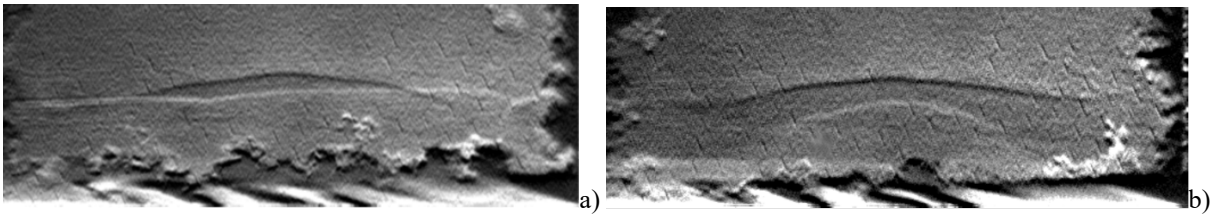
a) b)

Figure 9: Mie Scattering images demonstrating shock profiles generated during plasma actuation for (a) three filament and (b) single filament. Laser sheet is aligned with row 1 of pressure taps and ramp is in mid position.

4. Discussion

By combining information, from schlieren imaging, pressure data, and Mie scattering, a more complete description of the effect that plasma has on the shock train emerges. Near-adiabatic localized gas heating by the electrical discharge creates a subsonic region and volumetric expansion that causes a surrounding semi-conical shock wave and allows the existing nearby reflected shock to shift upstream. Figure 10 provides a visualization of this process for further clarification. With only a single filament turned on, the conical SW can be observed in both pressure data and Mie scattering images. With three filaments turned on, the conical SWs interfere due to cross flow pressure leveraging within the separation region/boundary layer and form a new, approximately-planar SW.

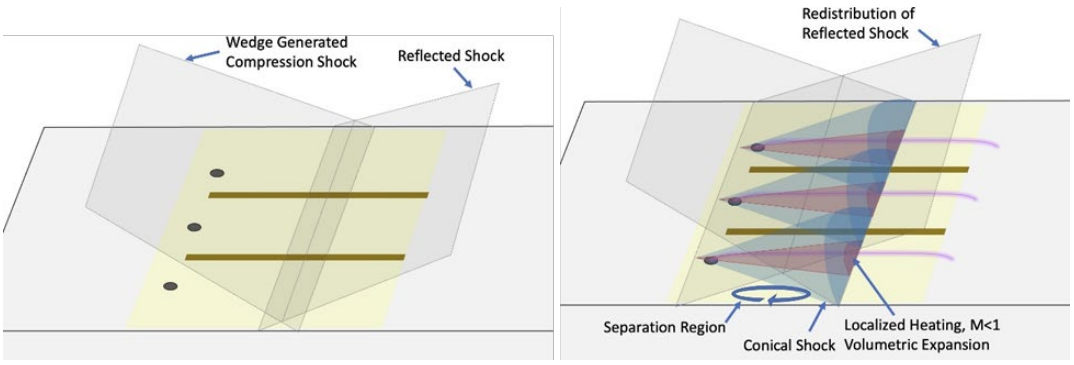

Figure 10: Illustration comparing shock structures with (a) plasma off and (b) plasma on

The important feature of the external SW interaction with the plasma-based displacement layer is that the reflected wedge-based SW is no longer strong and is detected as a very weak compression wave due to the pressure redistribution effect over an extended separation zone [30]. The second feature of this type of interaction is that the plasma-related SW is “amplified” by the impinging SW due to the pressure augmentation in the zone of plasma filaments.
Another important finding of this last test series is that the plasma power could be quite low (W_{pl}<1kW for each plasma filament) to achieve a valuable effect in the shock train redistribution. In reality, the plasma power is even lower than this because a significant portion of electrical power is released in heating the HV electrodes and heating the metallic

DOI: 10.13009/EUCASS2022-4848

wall where the plasma filaments are connected to. A simple estimate based on a previous measurements of the electrodes voltage drop [36], U_{el}≈100V, returns the power losses at electrodes to be around W_{el}≈0.5kW which makes the effectiveness of the SW control even more reasonable. The reduction of these power losses is an urgent technical task.

5. Summary

Previous studies [34, 31], which were conducted at Mach 2, used a multi-filamentary plasma to demonstrate pressure redistribution due to presence of longitudinal subsonic zones induced by each plasma filament. The current work provided experimental characterization of a single and a triple plasma filament interacting with an incoming shock wave. Mach 2 study demonstrated cross-flow surface pressure redistribution in vicinity of the plasma area and the impinging SW. In accordance with the model of interaction and the data acquired for a multi-filamentary patterned plasma array, a semi-cone shape of the plasma-induced SW was predicted with a zone of augmented pressure within that cone and a significantly lower pressure outside of it. This predicted effect was demonstrated experimentally by analysis of cross-flow pressure distribution for single and triple plasma filament configurations as well as through acetone Mie scattering visualization. The interference of individual semi-conical SWs resulting in a new plane SW setup is considered to be equivalent to shifting of the entire shock train upstream.
This technique demonstrates feasible potential for the control of shock wave – boundary layer interaction and, in general, a shock-dominated flows.

The authors would like to thank the US Air Force Office of Scientific Research (PM Dr. Gregg Abate) for funding this work, grant # FA9550-21-1-0006.

References

[1] J. L. Wagner, K. B. Yuceil, A. Valdivia, N. T. Clemens et D. S. Dolling, «Experimental investigation of unstart in an inlet/isolator model in Mach 5 flow,» *AIAA Journal,* vol. 47, #16, pp. 1528-1542, 2009.

[2] R. L. Klomparens, J. F. Driscoll et M. Gamba, «Unsteadiness characteristics and pressure distribution of an oblique shock train,» *AIAA Paper 2015-1519*, 2015.

[3] N. T. Clemens et V. Narayanaswamy, «Low-Frequency Unsteadiness of Shock Wave/Turbulent Boundary Layer Interactions,» *Annual Review of Fluid Mechanics,* vol. 46, pp. 14-46, 2014.

[4] K. Matsuo, Y. Miyazato et H. Kim, «Shock train and pseudoshock phenomena in internal gas flows,» *Prog. Aerosp. Sci.,* vol. 35, pp. 33-100, 1999.

[5] S. Schneider, «Effects of Roughness on Hypersonic Boundary-Layer Transition,» *J. of Spacecraft and Rockets,* vol. 45, #12, pp. 193-205, 2008.

[6] E. Reshotko et A. Tumin, «Role of Transient Growth in Roughness-Induced Transition,» *AIAA J.,* vol. 42, #14, p. 766–770, 2004.

[7] R. Hunt, J. F. Driscoll et M. Gamba, «Periodic forcing of a shock train in Mach 2.0 flow,» *AIAA Paper 2017-0088*, 2017.

[8] A. Weiss et H. Olivier, «Shock boundary layer interaction under the influence of a normal suction slot,» *Shock Waves,* vol. 24, pp. 11-19, 2014.

[9] A. Valdivia, K. B. Yuceil, J. L. Wagner, N. T. Clemens et D. S. Dolling, «Control of Supersonic Inlet-Isolator Unstart Using Active and Passive Vortex Generators,» *AIAA Journal,,* vol. 52, #16, pp. 1207-1218, 2014.

[10] H. Do, S. Im, M. Mungal et M. Cappelli, «The influence of boundary layers on supersonic inlet flow unstart induced by mass injection,» *Exp. Fluids,* vol. 51, pp. 679-691, 2011.

[11] H. Yan et D. Gaitonde, «Effect of Thermally Induced Perturbation in Supersonic Boundary Layers,» *Physics of Fluids,* vol. 22, pp. 064101(1-17), 2010.

[12] P. Bletzinger, B. N. Ganguly, D. Van Wie et A. Garscadden, «Plasmas in High Speed Aerodynamics,» *Journal of Physics D: Applied Physics,* vol. 38, #14, pp. R33-R57, 2005.

[13] D. Knight, «Survey of Aerodynamic Drag Reduction at High Speed by Energy Deposition,» *Journal of Propulsion and Power,* vol. 24, #16, p. 1153–1167, 2008.

[14] M. N. Shneider, S. O. Macheret, S. H. Zaidi, I. Girgis et R. B. Miles, «Virtual Shapes in Supersonic Flow Control with Energy Addition,» *Journal of Propulsion and Power,* vol. 24, #15, pp. 900-915, 2008.

DOI: 10.13009/EUCASS2022-4848

[15] A. Starikovskiy et N. Aleksandrov, Nonequilibrium Plasma Aerodynamics, Aeronautics and Astronautics, Max Mulder (Ed.): InTech, ISBN: 978-953-307-473-3, 2011.

[16] J. Poggie, T. McLaughlin et S. Leonov, «Plasma Aerodynamics: Current Status and Future Directions,» *ONERA Aerospace Lab Journal,* vol. AL10, #110, pp. 1-6, 2015.

[17] S. B. Leonov, I. V. Adamovich et V. R. Soloviev, «Dynamics of near-surface electric discharges and mechanisms of their interaction with the airflow, Topical Review,» *Plasma Sources Science and Technology,* vol. 25, #16, p. 20168, 2016.

[18] O. Azarova, «Supersonic Flow Control Using Combined Energy Deposition,» *Aerospace,* vol. 2, #11, pp. 118-134, 2015.

[19] V. Bityurin, A. Klimov, S. Leonov, D. V. Wie, V. Brovkin, Y. Kolesnichenko et A. Lutsky, «Effect of heterogeneous discharge plasma on shock wave structure and propagation,» *AIAA Paper 1999-4940,* https://doi.org/10.2514/6.1999-4940, 1999.

[20] O. A. Azarova, T. A. Lapushkina, K. V. Krasnobaev et O. V. Kravchenko, «Redistribution of Energy during Interaction of a Shock Wave with a Temperature Layered Plasma Region at Hypersonic Speeds,» *Aerospace,* vol. 8, #111, p. 326, 2021.

[21] D. Knight, Y. Kolesnichenko, V. Brovkin, D. Khmara, V. Lashkov et I. Mashek, «Interaction of Microwave-Generated Plasma with a Hemisphere Cylinder at Mach 2.1,» *AIAA Journal,* vol. 47, #112, pp. 2996-3010, 2009.

[22] S. Leonov, V. Bityurin, A. Klimov et Y. Kolesnichenko, «Influence of Structural Electric Discharges on Parameters of Streamlined Bodies in Airflow,» *AIAA Paper 2001-3057*, 2001.

[23] M. Samimy, N. Webb et A. Esfahani, «Reinventing the wheel: excitation of flow instabilities for active flow control using plasma actuators,» *J. Phys. D: Appl. Phys.,* vol. 52, p. 354002, 2019.

[24] J. Wang, Y. H. Li, B. Q. Cheng, C. B. Su, H. M. Song et Y. Wu, «Effects of plasma aerodynamic actuation on oblique shock wave in a cold supersonic flow,» *J. Phys. D: Appl. Phys,* vol. 42, #1165503, 2009.

[25] S. Quan, C. Bangqin, Y. Yonggui, L. Yiwen et J. Di, «A Study of Variation Patterns of Shock Wave Control by Different Plasma Aerodynamic Actuations,» *Plasma Science and Technology,* vol. 12, #16, p. 708, 2010.

[26] H. Yan, F. Liu, J. Xu et Y. Xue, «Study of Oblique Shock Wave Control by Surface Arc Discharge Plasma,» *AIAA Journal,* vol. 56, #12, pp. 532-541, 2018.

[27] Y. Watanabe, S. Elliott, A. W. Houpt et S. B. Leonov, «Q-DC Plasma Actuation for Mach-4 Supersonic Flow Control over Compression Ramp,» *AIAA Paper 2020-1889*, 2020.

[28] A. Houpt, B. Hedlund, S. Leonov, T. Ombrello et C. Carter, « Quasi-DC Electrical Discharge Characterization in a Supersonic Flow,» *Experiments in Fluids,* vol. 58, #14, p. 25, 2017.

[29] F. Falempin, A. Firsov, D. Yarantsev, M. Goldfeld, K. Timofeev et S. Leonov, «Plasma control of shock wave configuration in off-design mode of M = 2 inlet,» *Experiments in Fluids,* vol. 56, #154, 2015.

[30] S. B. Leonov, C. D. Carter, B. E. Hedlund, A. W. Houpt, T. Ombrello et A. A. Firsov, «Control of Amplitude and Position of Reflected Shock Wave by Stripwise Plasma,» *Paper AIAA 2018-0683*, 2018.

[31] S. Elliott, M. Hasegawa, H. Sakaue et S. Leonov, «Shock-Dominated Flow Control by Plasma Array: Pressure Analysis Including Pressure-Sensitive Paint Visualization,» *Experimental Thermal and Fluid Science,* vol.131, # 110522, 2022.

[32] S. B. Leonov et D. A. Yarantsev, «Control of separation phenomena in high-speed flow by means of the surface electric discharge,» *Fluid Dynamics,* vol. 43, #16, pp. 945-953, 2008.

[33] Y. Watanabe, S. Elliott, A. Firsov, A. Houpt et S. Leonov, «Rapid control of force/momentum on a model ramp by quasi-DC plasma,» *J. Phys. D: Appl. Phys.,* vol. 52, #144, p. 444003, 2019.

[34] S. Elliott, P. Andrews, P. Lax et S. B. Leonov, «Control of Shock Positions in a Supersonic Duct by Plasma Array,» *AIAA Paper 2022-2553,* 2022.

[35] P. Andrews, P. Lax, S. Elliott, A. Firsov et S. Leonov, «Flow Characterization at Heated Air Supersonic Facility SBR-50,» *Fluids,* vol. 7, #15, p. 168, 2022.

[36] A. Efimov, A. Firsov, N. Kolosov et S. B. Leonov, «Characterization of electric discharge collocated with gas jet in supersonic airflow,» *Plasma Sources Science and Technology,* vol. 29, #17, p. 07LT01, 2020.